Light Scattering Studies of Hi-Impact Polystyrene

R. J. TABAR, S. R. HU, and R. S. STEIN,* *Polymer Research Institute, University of Massachusetts, Amherst, Massachusetts 01003*

Synopsis

Small-angle light scattering techniques have been used to evaluate the factors controlling the transparency of two hi-impact polystyrene films. These factors were found to include surface smoothness, volume fraction of the phases in the system, the difference of the refractive indices of the phases, and the sizes of the phases. The elongation of the rubber phase during processing was also determined.

INTRODUCTION

The optical clarity of polymer films has great significance in many commercial applications of polymers. Optical clarity may be esthetically desirable for such applications as beverage containers and food wrappers. It is a necessity for applications such as safety face shields and windows.

While films made from single phase amorphous polymers are generally clear, such films may be unsatisfactory for certain applications due to other inadequacies such as brittleness, low glass transition temperature, poor aging characteristics, expense of production, etc. One can often achieve the other necessary properties in a polymer film with a polyphase polymer system such as a phase separated polymer blend or a semicrystalline polymer. These polyphase systems generally suffer from lack of optical clarity. Optical clarity can be improved in these systems by close control of such factors as the refractive index of the phases, the size and orientation of the phases, and the surface smoothness of the film.

This paper discusses the importance of these factors in achieving optical clarity and outlines the manner in which they should be controlled. Two commercially available films made from polyphase blends are evaluated for optical clarity. The contributing factors responsible for their degree of clarity (transparency) are evaluated by small-angle light scattering (SALS).

EXPERIMENTAL

The samples were obtained from two nine ounce disposable beverage cups, referred to as samples 1 and 2. The cups are made of rubber-modified polystyrene compositions. Three specimens (approximately 6 × 15 mm) were cut from different positions in each cup, as described in Figure 1.

Silicone oil was applied to the surface of the samples for the light scattering tests to minimize surface scattering effects. Past experience indicates that this procedure is quite effective in supressing surface scattering. However, in view

* To whom correspondence should be sent.

Journal of Applied Polymer Science, Vol. 28, 1409–1420 (1983)
 CCC 0021-8995/83/041409-12$02.20

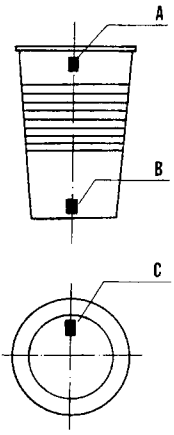

Fig. 1. Diagram of the positions of the A-, B-, and C-position specimens in the beverage cups.

of the large contribution to surface scattering evident from Table I, there is some possibility that there is some residual surface scattering contributing along with the internal scattering for the oil-wetted films. A procedure which could be employed to test this effect (which was not done) would be to determine the scattering pattern as a function of the refractive index of the oil. The light scattering was performed using a 2-dimensional position sensitive detector described elsewhere.[1] Photographs of the light scattering patterns were also obtained. The light transmission was measured, with and without silicone oil, using a photometer arranged to collect all of the light energy emitted at scattering angles less than 2 mrad. All the light sources used were He–Ne lasers (wavelength = 632.8 nm), and no polarizers were used.

RESULTS

Transmittance

The light transmittances for the six specimens, with and without silicone oil in the surfaces, are given in Table I. It can be seen from these results that sample 1 is more transparent in the "as received" condition than sample 2. It can also be seen that the transparency of both samples is greatly enhanced by the silicone oil, indicating that there is a significant amount of surface scattering by both samples. Sample 1 has greater transparency than sample 2 for the oil-covered samples, except for the A-position specimens.

TABLE I
Light Transmittance at λ = 632.8 nm (Aperture Size = ±2 mrad)

Specimen	Transmittance as received (%)	Transmittance with silicone oil (%)
1-A	2	28
2-A	1	37
1-B	15	33
2-B	1	3
1-C	2	5
2-C	1	2

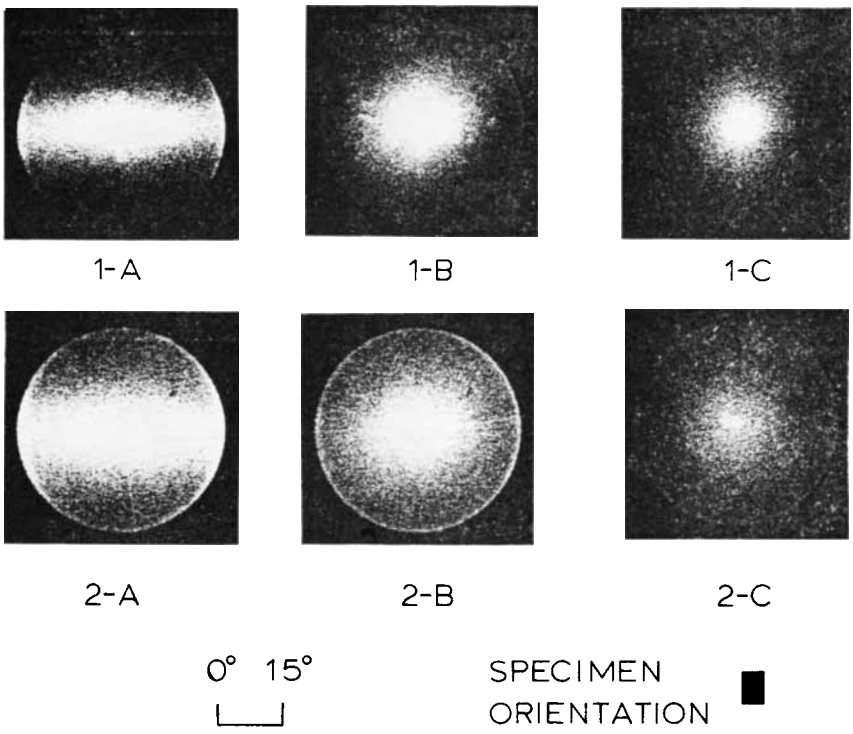

Fig. 2. Photographic light scattering patterns from samples 1 and 2, A-, B-, and C-position specimens. The exposure conditions are the same for the A- and B-position specimens. The two C-position specimens have the same exposure conditions, but different from the A- and B-positions.

Photographic

Photographic light scattering patterns from the six specimens are presented in Figure 2. The same photographic conditions were used for the A- and B-position specimens. The same photographic conditions were used for both C-position specimens, but these conditions differed from those for the A- and B-position specimens. Therefore, qualitative intensity comparisons can be made between samples 1 and 2 for any one specimen position.

The A-position specimen patterns are elongated in the horizontal direction, indicating elongation of the scattering structures in the vertical direction (the vertical direction in an upright sitting cup). This orientation is probably a result of the forming process of the cups. The intensity levels of the two A-position specimen patterns appear qualitatively similar.

The B- and C-position specimen patterns appear to be circularly symmetric, indicating no preferred orientation of the scattering structures in these specimens. It is apparent that sample 1 has greater low angle scattering (i.e., greater transparency) than sample 2 for both the B- and C-position specimens.

Position-Sensitive Detector

Light scattering data from the six specimens obtained on the 2-dimensional position-sensitive detector are given in Figures 3–5. [The scattering vector

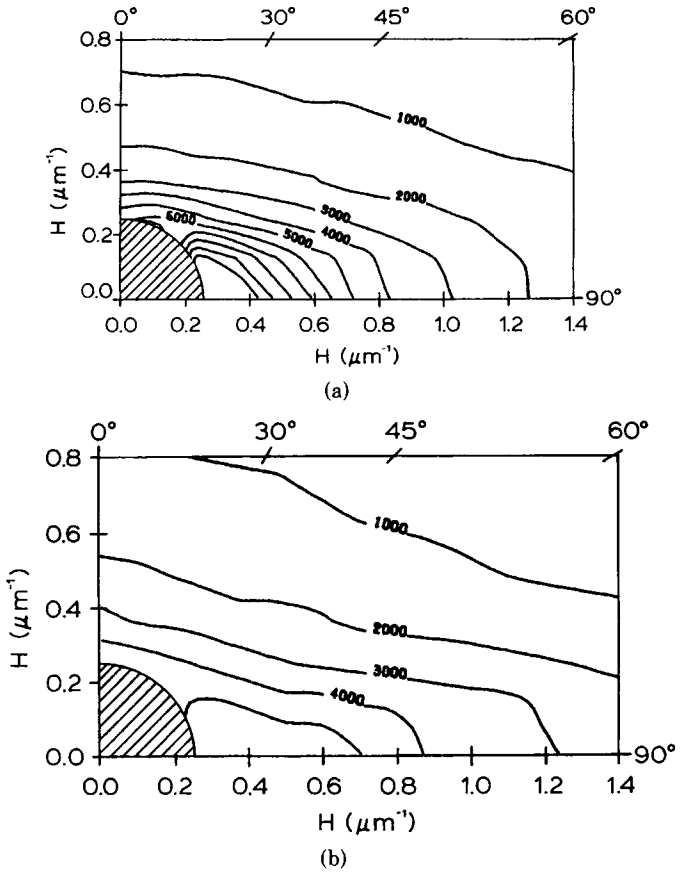

Fig. 3. Two dimensional, single quadrant averaged light scattering intensity contours from the A-position specimen. Main beam stop is indicated by the hatched area: (a) sample 1-A, contours of every 1,000 intensity units; (b) sample 2-A, contours at every 1,000 intensity units.

magnitude $H = (4\pi/\lambda) \sin \theta/2$, where λ is the wavelength of the light in the sample and θ is the polar scattering angle in the sample.] The four quadrant scattering patterns have been averaged into single quadrant patterns. Isointensity contours are shown for each specimen's scattering pattern. The main beam was suppressed within the hatched areas in Figures 3–5. The experimental conditions are such that the intensities can be compared between samples (1 and 2) for any one specimen position (A, B, or C).

The light scattering contours give quantitative confirmation of the results concluded from the photographic studies: the A-position specimens show structural elongation in the vertical direction, the B- and C-position specimen patterns are approximately circularly symmetric, sample 1 shows higher intensity levels of scattering, for the B- and C-position specimens, at all angles measured.

The light scattering contours have been analyzed in the Guinier method[2] at various azimuthal angles. At small angles, random two-phase systems follow the general scattering behavior of

$$I(H) = I(0) \exp(- R_g^2 H^2/3) \quad (1)$$

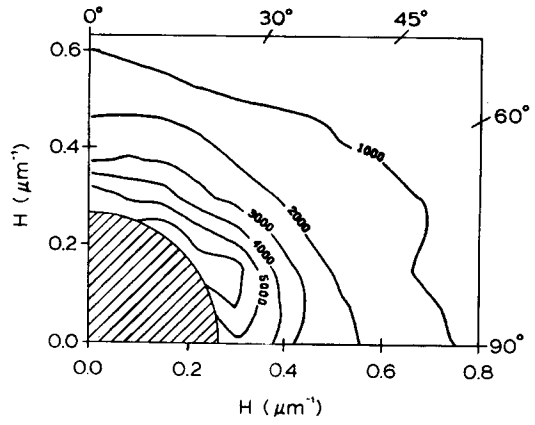

(a)

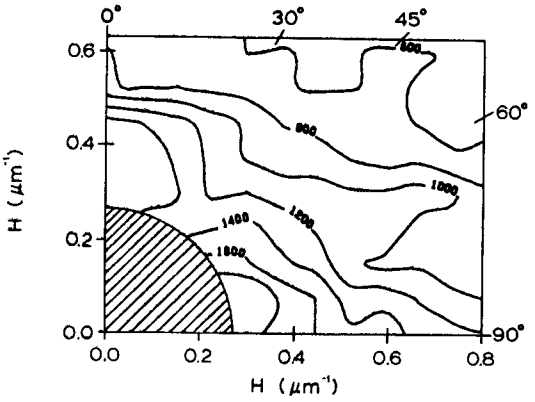

(b)

Fig. 4. Two-dimensional, single quadrant averaged light scattering intensity contours from the B-position specimen. Main beam stop is indicated by the hatched area: (a) sample 1-A, contours at every 1,000 intensity units; (b) sample 2-A, contours at every 200 intensity units.

where $I(H)$ is the scattered intensity at scattering vector magnitude H, $I(0)$ is the extrapolated intensity at $H = 0$, and R_g is the average radius of gyration of the inhomogeneities. Equation (1) can be rearranged to give

$$\ln I(H) = \ln I(0) - R_g{}^2H^2/3 \tag{2}$$

Therefore a plot of $\ln I(H)$ vs. H^2 gives a straight line at small H values with a slope $= -R_g{}^2/3$ and an intercept of $\ln I(0)$.

The intensity at zero angle is given by[3]

$$I(0) = K\langle\eta^2\rangle V \tag{3}$$

where K is a constant, $\langle\eta^2\rangle$ is the mean squared fluctuation in the refractive index, and V is the average volume of the inhomogeneities ($V \sim R_g{}^3$). For random two-phase systems with sharp boundaries[4,5]

$$\langle\eta^2\rangle = \phi_1\phi_2(n_1 - n_2)^2 \tag{4}$$

where ϕ_1 and ϕ_2 are the volume fractions of phases 1 and 2 and n_1 and n_2 are the refractive indices of phases 1 and 2, respectively. $I(0)$ can then be given as

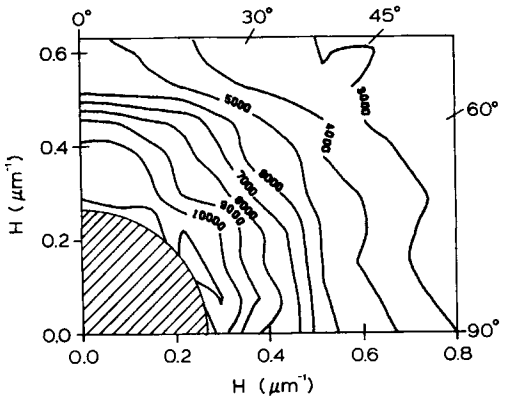

(a)

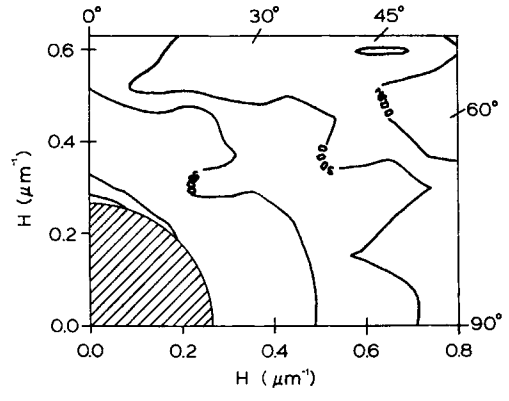

(b)

Fig. 5. Two-dimensional, single quadrant averaged light scattering intensity contours from the C-position specimen. Main beam stop is indicated by the hatched area: (a) sample 1-C, contours at every 1,000 intensity units; (b) sample 2-C, contours at every 500 intensity units.

$$I(0) = K'\phi_1\phi_2(n_1 - n_2)^2 R_g{}^3 \tag{5}$$

where K' is a new constant. Since $R_g{}^2$ is determined from the slope of the plot of $I(H)$ vs. H^2, a term proportional to the mean-squared fluctuation can be determined from the size-corrected intercept according to

$$I(0)/R_g{}^3 = K'\phi_1\phi_2(n_1 - n_2)^2 = K'\langle\eta^2\rangle \tag{6}$$

The average R_g and $I(0)/R_g{}^3$ were determined from the SALS data for the six specimens.

For the A-position specimens, radii of gyration in both the vertical and horizontal directions can be determined. The vertical radius of gyration ($R_{g\parallel}$) is determined from eq. (2) using intensity values at an azimuthal angle of 0°. The horizontal radius of gyration ($R_{g\perp}$) is determined using intensity values at an azimuthal angle of 90°.

The elongation ratio in the stretching direction ($\epsilon_\parallel$) can be defined as

$$\epsilon_\parallel = R_{g\parallel}/R_{g0} \tag{7}$$

where R_{g0} is the average radius of gyration of the particles in the unstrained state. Similarly, the elongation ratio in the transverse direction ($\epsilon_\perp$) is given by

$$\epsilon_\perp = R_{g\perp}/R_{g0} \tag{8}$$

For cylindrical symmetry and constant volume during deformation, $\epsilon_\parallel$ and $\epsilon_\perp$ are related as

$$\epsilon_\perp = \epsilon_\parallel^{-1/2} \tag{9}$$

Combination of eqs. (6), (7), and (8) leads to a relationship between the radii of gyration determined by light scattering and the particle elongation

$$R_{g\parallel}/R_{g\perp} = \epsilon^{3/2} \tag{10}$$

The light scattering profiles for azimuthal angles 0° and 90° are given in Figure 6 for samples 1 and 2, A-position specimen. The linear regression lines indicated are for the low H range of the data. The size-corrected intercepts, radii of gyration, and elongation of the A-position specimens are summarized in Table II.

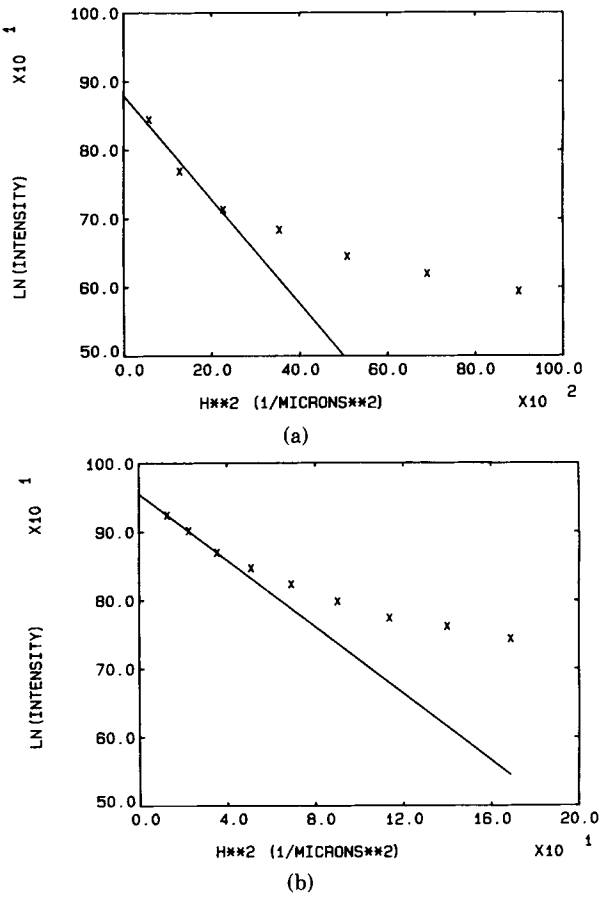

Fig. 6. Guinier type light scattering plots from the A-position specimen: (a) sample 1-A, azimuthal angle = 0°; (b) sample 1-A, azimuthal angle = 90°; (c) sample 2-A, azimuthal angle = 0°; (d) sample 2-A, azimuthal angle = 90°.

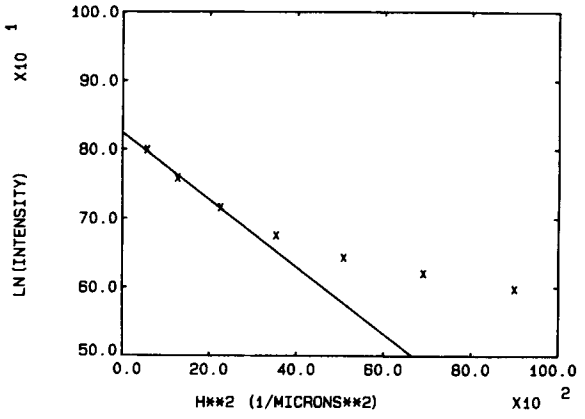

(c)

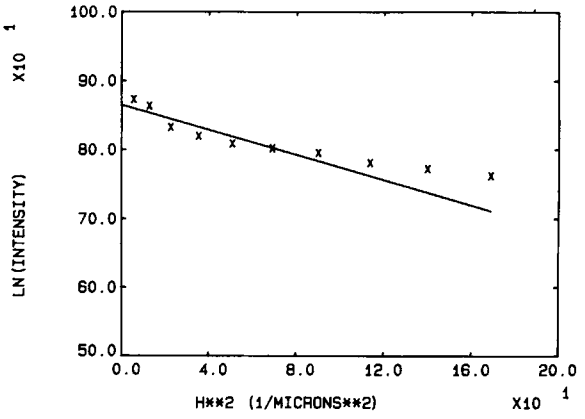

(d)

Fig. 6 (*Continued from the previous page.*)

The radii of gyration listed in Table II indicate a larger particle size in both azimuthal directions for sample 1 as compared to sample 2. Sample 2 seems to show a slightly higher elongation ratio than sample 1. The size-corrected intercept values are higher for sample 2 for each azimuthal angle.

B- and C-position specimens give approximately circularly symmetrical light scattering patterns (Figs. 4 and 5). The light scattering data was therefore circularly averaged and then analyzed according to eqs. (2) and (6). The Guinier plots of the circularly averaged data are given in Figure 7. Table III summarizes this data. It is clear that sample 1 exhibits larger particle size than sample 2. Also sample 2 has equal or greater size-corrected intercept values for these B- and C-position specimens.

TABLE II
Guinier Analysis of Specimen Type A (Fig. 6)

Sample	$R_{g\parallel}$ (μm)	$R_{g\perp}$ (μm)	$\epsilon_{\parallel}$	$I(0)/R_{g\parallel}{}^3$	$I(0)/R_{g\perp}{}^3$
1	4.8	2.7	1.5	61	720
2	3.8	1.7	1.7	68	1300

DISCUSSION

Sample 1 is more transparent than sample 2 for each specimen type in the "as received" condition. The light scattering studies can be used to analyze the reason for the transparency and to suggest means of controlling the transparency of such films. It is apparent from the transmission data from the oil-covered samples that control of surface smoothness may be a very significant means of improving the transparency of polyphase films. This conclusion is similar to the results of Stehling et al.[6] They concluded that most of the haze of low-density polyethylene was due to surface scattering.

The greater transparency of sample 1 can be analyzed in terms of the SALS results. The greater transparency of sample 1 may be due to its larger particle size. Although one generally associates larger particle size with greater haze, this may not be true for sufficiently large particles.

If one considers haze to be that portion of the scattered light scattered at angles greater than some minimum angle θ_{min}, then it has recently been shown[7] that haze does not continue to increase with increasing particle size. For a given wavelength of light and $\theta_{min} > 0$, there exists a critical inhomogeneity size, a_c,

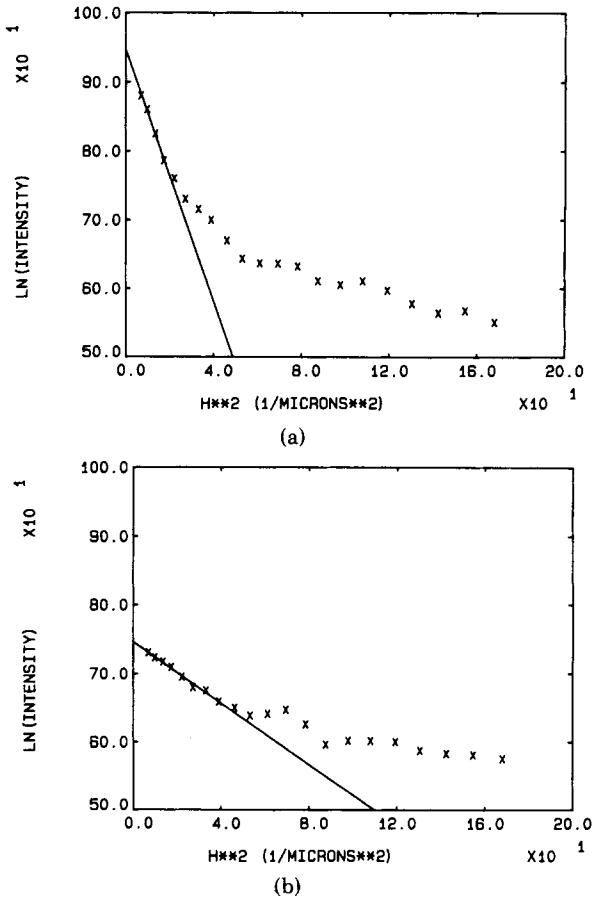

Fig. 7. Guinier type plots from circularly averaged light scattering data: (a) sample 1-B; (b) sample 2-B; (c) sample 1-C; (d) sample 2-C.

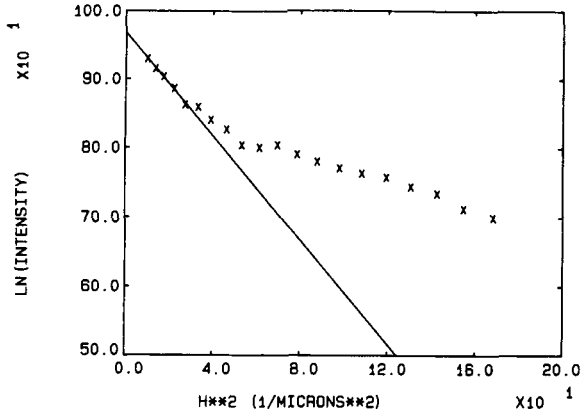

(c)

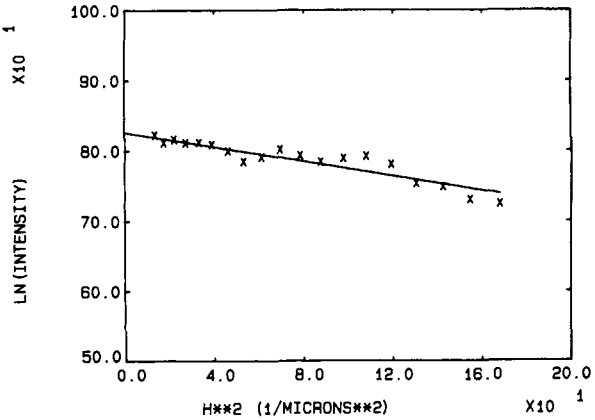

(d)

Fig. 7 (*Continued from the previous page.*)

where the haze has a maximum as a function of a. For reasonably small minimum angle values ($\theta_{min} < 7°$), a_c is given by

$$a_c H_{min} = 1.0 \tag{11}$$

where $H_{min} = (4\pi/\lambda) \sin(\theta_{min}/2)$. It should be noted that the ASTM standard test[8] for haze from polymers specifies $\theta_{min} = 2.5°$. Equation (11) is for a monochromatic radiation. The critical size for "white light" should be derived by accumulating the effects of wavelength over the visible spectrum.[7]

TABLE III
Guinier Analysis of A- and B-Position Specimens (Fig. 7)

Specimen	R_g (μm)	$I(0)/R_g^3$
1-B	5.2	91
2-B	2.6	100
1-C	3.4	420
2-C	1.2	2000

It appears that in our systems we may be beyond the critical value of a such that the systems with the larger inhomogeneities have a greater transparency. Since the radius of gyration determined by scattering is weighted towards the larger radii of gyration,[2] the scattering will be sensitive to the distribution of the sizes of the inhomogeneities as well as the average size.

Apparently, the B-position specimens have a larger particle size than the C-position specimens from the same sample number. The Guinier analysis used assumes spherically symmetrical particles. The size difference could be due to the particles in the B-position specimens being oblate spheroids in the plane of the film, being thinner in the direction perpendicular to the film than the C-position specimens. Such a shape difference would allow the B- and C-position particles to have the same volume, but different R_g as measured by SALS.

To examine the possibility of such a shape change, similar SALS experiments were performed on samples which were tilted 45° relative to the incident beam. There was no apparent elongation of the SALS patterns due to the tilting. Tilting of oblate spheroids would produce an elongated pattern. The size difference between B- and C-position specimens may be due to different phase growth for the different specimens due to the different thermal and mechanical history of the two different positions in the cups during their molding.

The intensity of the SALS is also dependent upon the value of $\langle \eta^2 \rangle$. The size-corrected intercept values reported in Tables II and III are proportional to $\langle \eta^2 \rangle$. The results show that the size-corrected intercepts for sample 2 are equal to or larger than those for sample 1, indicating that $\langle \eta^2 \rangle$ is larger for sample 2 than sample 1. The larger value of $\langle \eta^2 \rangle$ for sample 2 may be due to a larger volume fraction of rubber particles or a larger refractive index difference between the two phases in sample 2 as compared to sample 1. Since we have no further information on these systems, we cannot distinguish between these two effects. The greater transparency of sample 1 may be due to its lower value of $\langle \eta^2 \rangle$ alone or it may also be due to the larger inhomogeneity size. Our data does not allow us to decide whether the larger $\langle \eta^2 \rangle$ values of sample 2 is sufficient to cause its greater scattering or if the size effect is also important.

CONCLUSIONS

This study has demonstrated the use of SALS techniques and a 2-dimensional position-sensitive light scattering detector to evaluate the cause of transparency in very practical polyphase systems. The principal factors found to be affecting the transparency of these hi-impact polystyrene products are the surface roughness, the volume fractions of the phases, the difference of the refractive indices of the phases, and the size of the phases. The thickness of the material is also important. The control of these factors in the manufacturing of these products should lead to the control of the transparency of these products. The extension of the inhomogeneities due to processing were also determined by these techniques.

We acknowledge the participation of the Monsanto Company in providing samples and in discussions relevant to this study. The work was supported in part by grants from the National Science Foundation and the Materials Research Laboratory of the University of Massachusetts.

References

1. R. J. Tabar, M. B. Long, and R. S. Stein, *J. Polym. Sci., Polym. Phys. Ed.*, to appear.
2. A. Guinier and G. Fournet, *Small-Angle Scattering of X-Rays*, Wiley, New York, 1955.
3. P. Debye and A. M. Bueche, *J. Appl. Phys.*, **20,** 518 (1949).
4. R. S. Stein, *Rubber Chem. Technol.*, **49,** 458 (1976).
5. J. T. Koberstein, T. P. Russell, and R. S. Stein, *J. Polym. Sci., Polym. Phys. Ed.*, **17,** 1719 (1979).
6. F. C. Stehling, C. S. Speed, and L. Westerman, *Macromolecules*, **14,** 698 (1981).
7. R. J. Tabar and R. S. Stein, to appear.
8. "Standard Test Method for Haze and Luminous Transmittance of Transparent Plastics," ASTM D1003, *1980 Annual Book of ASTM Standards*, Part 35, American Society for Testing and Materials, Easton, Md., 1980.

Received July 15, 1982
Accepted November 29, 1982